DESIGN AND CHARACTERIZATION OF NANOELECTROMECHANICAL SWITCHES

A Thesis

Presented to the Faculty of the Graduate School

of Cornell University

In Partial Fulfillment of the Requirements for the Degree of

Master of Science

by

Susmita Bhandari

August 2009

ABSTRACT

With the scaling down of electromechanical switches to from micro- to nano-scale, short-range forces like Casimir and van der Waals become more influential. These short range forces can significantly modify the static and dynamic behavior of the switches. In this study, the influence of these short-range forces on cantilever and fixed-fixed type nanoelectromechanical (NEM) switches are investigated. Results from analytical and finite element modeling show that the pull-in parameters and the switching and release behaviors of compliant switches are more affected by the short-range forces. Dynamic simulations show that NEM switches are vulnerable to stiction. Using smart geometry and electrode configurations it is possible to overcome stiction at the expense of a more complex design and higher pull-in voltage. Finally a memory element and electric field sensor are discussed as promising applications of these switches.

BIOGRAPHICAL SKETCH

Susmita Bhandari received the B.S. degree in Engineering from Trinity College, CT in 2007. That same year she started her graduate studies at Cornell University, NY. Her research at Cornell has focused on microelectromechanical systems (MEMS) in general and inertial sensors and radio frequency micro- and nano-electromechanical switches in particular.

ACKNOWLEDGEMENTS

I sincerely thank my thesis advisor Prof. Sunil A. Bhave and special committee member Prof. Edwin C. Kan for their assistance and support. I appreciate OxideMEMS group members for their help during the last two years. Finally, I thank Bozidar Marinkovic for his encouragement and unconditional support.

I am very grateful to the department of Electrical and Computer Engineering, Cornell University and Irwin and Joan Jacobs for awarding me the Jacobs Fellowship during my first year here at Cornell.

TABLE OF CONTENTS

Page

BIOGRAPHICAL SKETCH……iii

ACKNOWLEDGEMENTS……...iv

LIST OF FIGURES……...vi

LIST OF TABLES…….....vii

CHAPTER

1. INTRODUCTION……..1

2. BEAM STATICS……...4

Theory……4

Results and Discussion.…….……..……..9

3. BEAM DYNAMICS…….16

Theory……...16

Switching Time: Results and Discussion…….....17

Release Time: Results and Discussion……..20

4. APPLICATIONS……..24

Dynamic Random Access Memory (DRAM)…….....24

DRAM: Results and Discussion……...24

Electric Field Sensor…….27

Electric Field Sensor: Results and Discussion……..31

5. CONCLUSION…….34

APPENDIX……...36

Material Properties……36

Numerical Constants…….37

REFERENCES……..38

LIST OF FIGURES

FIGURE Page

1. Illustration of a single degree of freedom (SDOF) lumped model…..…….7
2. Comparison between analytical and FEM models……..11
3. Parametric analysis of pull-in voltage using analytical model……13
4. Effect of fringing field in the analytical model……...14
5. Dynamic pull-in response without Casimir force…….....18
6. Dynamic pull-in response with Casimir force……19
7. Effect of applied voltage on the switching time…….20
8. Dynamic pull-out response without short-range forces……..21
9. Dynamic pull-out response with short-range forces……...22
10. 3D model of NEM DRAM cell……...24
11. Parametric analysis of pull-in voltage using FEM model……...25
12. Dynamic pull-out response of NEM DRAM memory cell…….26
13. The concept of the hybrid NEMS-antenna based electric field sensor……...28
14. Frequency response of the PZT NEM resonator…….31
15. Parametric analysis of signal to noise ratio…….32
16. Frequency response of an ideal PZT resonator design……....33

LIST OF TABLES

TABLE Page

1. Release response of cantilever beam showing switching time……...26

2. Proprietary material properties…...……36

3. Silicon material properties……..36

4. PZT material properties……..37

5. List of numerical constants…….37

CHAPTER 1

INTRODUCTION

Electrostatically actuated micro-electro-mechanical system (MEMS) based devices have been around for a long time. MEMS switch for instance is widely used in RF applications because it offers small insertion loss when 'on' and high isolation when 'off', characteristics that are ideal for high frequency communication. Nano-electro-mechanical system (NEMS) is an extension of the MEMS devices scaled down to the nanometer range. NEM switches are the fundamental building blocks of many NEMS based devices. A typical NEM switch consists of two electrodes, one of which is movable while the other is fixed. A voltage difference between the two electrodes causes the movable electrode to deflect towards the fixed electrode because of electrostatic attraction. Beyond a certain applied voltage, the movable electrode loses stability and the gap between the electrodes decreases rapidly until they come into contact with each other. This instability is called the pull-in phenomenon and the displacement and voltage at which it occurs are the pull-in parameters.

Ostenberg and Senturia have derived an analytical expression for the pull-in parameters of the MEM switch in [1]. Bochobza-Degani and Nemirovsky have presented calculation of the pull-in parameters using a lumped two degrees of freedom model in [2]. These basic models have been developed considering only ideal electrostatic actuation. However, with decreasing gap between the electrodes, surface forces [3] such as van der Waals interaction become more important than the body forces in determining the static and dynamic behavior of NEM switches. There are two main surface based forces that become significant in nano-scale and have to be considered when the electrodes of NEM switch come to a close contact. The first is the van der Waals force which is the result of the interaction between instantaneous dipole moments of atoms and second one is the Casimir force which is the result of the

random vacuum fluctuations. Since these forces usually act over small distances of several nanometers, they are commonly referred to as short-range forces.

Desquenes et al. studied the effect of van der Waals force on the pull-in voltage while neglecting its effect on the pull-in gap in [4]. Rotkin considered the influence of van der Waals force on the pull-in gap and obtained analytical expressions for the pull-in parameters using a general model in [5]. Stiction in MEMS due to van der Waals force has also been studied extensively and a theoretical model was presented by van Spengen et al. in [6]. Lin and Zhao have studied the dynamic behavior of nanoscale electrostatic actuators by considering the effect of van der Waals force using a one degree of freedom lumped parameter model in [7]. Ramezani et al. have studied the effect of the van der Waals force on the pull-in parameters of cantilever type nanoscale electrostatic actuators using distributed parameter model in [8].

The attractive Casimir force, [9] first predicted by Hendrik Casimir, between two objects placed close together is a quantum mechanical effect that is significant in NEM switches. Serry et al. studied the effect of Casimir force in MEMS in [10] and Chan et al. measured the Casimir force in [11]. It was Chan et al. again who used a torsional MEMS actuator to demonstrate the existence of Casimir force in [12]. Lin and Zhao have studied the Casimir effect on the pull-in parameters of NEM switches using one degree of freedom lumped parameter model in [13].

A study where both van der Waals and Casimir forces are included is needed since both of these forces have separately been shown to have significant effect on the behavior of NEM switches. Such a model that includes these short-range forces will be useful in designing the next generation NEM switches with more accurate pull-in voltages, switching times and robustness to stiction. Moreover, the fringing field effect should also be considered for a more accurate determination of the pull-in parameters.

In this thesis, the effect of van der Waals, Casimir and fringing electrostatic forces on the pull-in parameters of cantilever and fixed-fixed type NEM switches are investigated in detail. Analytical expressions for the pull-in parameters have been derived for uniform load conditions using a single degree of freedom (SDOF) lumped model for both cantilever and fixed-fixed type switches. These analytical equations can be solved numerically to determine the pull-in parameters. The analytical results are compared to simulations based on finite element analysis using COMSOL Multiphysics software. Since, many applications of NEM switches are sensitive to switching frequency, dynamic analysis is also performed for the two types of beams to estimate switching and release times, and also the behavior of the switch as it pulls in or releases. Lastly, two potential applications of NEM switches that are receiving much attention in the NEMS world are discussed.

CHAPTER 2

BEAM STATICS

As device dimensions are reduced to micro- and nano-scales, the ratio of the volume of the device to its surface area is drastically reduced causing the surface forces to dominate over body forces. The atomistic surface forces that are important in NEM switches include long-range electrostatic or columbic force and short-range van der Waals and Casimir forces. Quantum effects in the form of Casimir force and van der Waals molecular interaction are commonly attributed to in-use stiction in MEM and NEM devices. Moreover, these forces play an important role, particularly in the nano regime, in determining the device pull-in parameters.

Theory

First discovered by Hendrik Casimir in 1948, Casimir force is the mechanical effect of randomly fluctuating electromagnetic fields in the vacuum. When two plates are positioned close together electromagnetic fields are reflected back and forth in the cavity between the plates, with fields at integer multiple of half the wavelength receiving amplification resulting in 'cavity resonance', while others getting attenuation. Since fields carry energy, they exert pressure on the surface of the plates, commonly known as radiation pressure. At cavity resonance the radiation pressure within the cavity is greater than outside causing the plates to move apart. Out of resonance, the plates move closer together. However, on average the attractive force has a greater impact and thus the net effect of the Casimir force is attractive causing the plates to move towards each other [14]. The attractive Casimir force between two parallel plates with surface area A separated by a distance r is given by [15]:

$$F_C(r) = -\frac{\delta U}{\delta r} = -\frac{\delta}{\delta r}\left(\frac{\pi^2 \hbar c A}{720 r^3}\right) = \frac{\pi^2 \hbar c A}{240 r^4} \tag{1}$$

where, U is potential energy, $\hbar$ is Planck's constant divided by 2π and c is the speed of light in vacuum[1].

Surface adhesion in a completely waterless environment has long been associated with van der Waals force. This molecular level interaction has three regimes of operation. When distance is larger than 20nm, it is in the retardation region (d_{ret}) and when distance is smaller than a cut-off (d_{co}) of typically 0.165nm, it is in the repulsive region. Only for the range of distances between d_{ret} and d_{co} is the force contribution attractive. Since for NEM switches, the gaps are nominally at least two orders of magnitude higher than the cut-off, only the attractive component of van der Waals force is important for static analysis. However, in dynamic analysis the repulsive component of the force should be included because it can contribute to the bouncing of the beam and therefore affect the settling time. The two components of van der Waals force F_{vdW} also known as Lennard-Jones force is given by:

$$F_{vdW}(r) = \left.\frac{A_{Ham}A}{6\pi r^3}\right|_{d_{co} < r < d_{ret}} + \left.\frac{C_2 A}{r^9}\right|_{r < d_{co}} \tag{2}$$

where A_{Ham} is the Hamaker constant and C_2 is the repulsive constant.

NEM switches are commonly actuated via the electrostatic actuation whereby a potential difference V is applied across two electrodes. The resulting attractive electrostatic force F_{elec} in vacuum between two plates is equal to:

$$F_{elec}(r) = \frac{\varepsilon_o A V^2}{2r^2} \tag{3}$$

where ε_o is the permittivity of free space.

The spring restoring force F_{res} which counteracts the contributions from the attractive forces is expressed as:

[1] All the numerical constants are listed in the appendix.

$$F_{res}(r) = k(g_o - r) \tag{4}$$

where k is the lumped element spring constant of a beam and g_o is the initial gap between the movable and fixed electrodes. The spring constant is determined from Euler-Bernoulli beam theory [16] and is dependent on beam geometry, the boundary condition at beams ends, type of force loading and force distribution applied across the beam and the material properties. In this particular case, the spring constant of a cantilever k_{CL} and that of a fixed-fixed beam k_{FF} are given below:

$$k_{CL} = \frac{8EI}{L^3} \qquad k_{FF} = \frac{384EI}{L^3} \tag{5}$$

where, E is the Young's modulus of the structural material[2], I is the moment of inertia and L is the length of the beam.

Figure 1 below shows the SDOF lumped model that considers all the forces discussed above. Here the beam is modeled as a parallel plate capacitor with one movable electrode. The restoring force in the movable electrode is modeled as a mechanical spring. It is important to note that this model assumes the two plates of the capacitor remain parallel as they move closer together. In reality, the beams will change shape as they get pulled-in closer to the substrate effectively reducing the area over which the short-range forces are acting. Nevertheless, this SDOF analytical model is still expected to predict the general behavior of the beams correctly. To verify the effect of this assumption, full three-dimensional (3D) simulations are performed using the finite element modeling (FEM) software COMSOL.

[2] The structural material used is proprietary. All the material properties are given in the appendix.

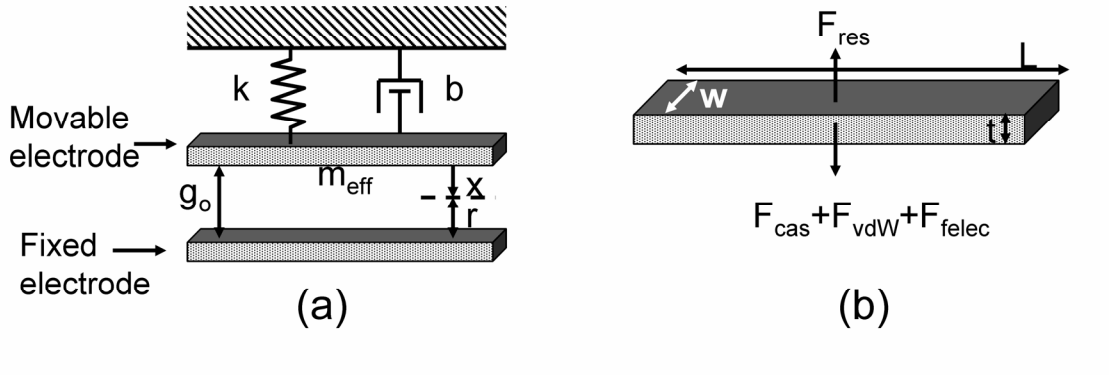

Figure 1: Illustration of a single degree of freedom (SDOF) lumped model. (a) Model of a parallel plate electrostatic actuator. (b) Free body diagram showing all the forces.

While the attractive forces increase nonlinearly with displacement, the spring restoring force has a linear relationship with it. By setting the sum of all the forces acting on a beam to zero it can be shown that there exists a critical displacement (g_{pi}). For beam displacements smaller than $g_{pi,}$ the forces will be in stable equilibrium. However, when the displacement exceeds g_{pi}, the attractive forces dominate over the restoring force causing instability and subsequent collapse of the beam. This phenomenon is known as the pull-in condition. The critical displacement also has a corresponding voltage value called the pull-in voltage (V_{pi}).

Traditionally the pull-in model includes only the electrostatic force and the spring restoring force. Setting the sum of these two forces to zero we get:

$$F_{net}(r) = \frac{\varepsilon_o A V^2}{2r^2} - k(g_o - r) = 0 \tag{5}$$

The second condition for stable equilibrium is when $\partial F_{net}(r)/\partial r < 0$. Using the critical condition $\partial F_{net}(r)/\partial r = 0$ and equation (5) we obtain:

$$g_{pi} = \frac{2}{3} g_o \tag{6}$$

$$V_{pi} = \sqrt{\frac{8kg_o^3}{27\varepsilon_o A}} \tag{7}$$

When Casimir and van der Waals forces are considered, the expression for net force changes and the revised equation is given as follows:

$$F_{net}(r) = \frac{\pi^2 \hbar c A}{240 r^4} + \frac{A_{Ham} A}{6\pi r^3} + \frac{\varepsilon_o A V^2}{2r^2} - k(g_o - r) = 0 \tag{8}$$

Applying the same equilibrium condition ($\partial F_{net}(r)/\partial r = 0$) to equation (8) yields:

$$-\frac{\pi^2 \hbar c A}{120 r^4} - \frac{\varepsilon_o A V^2}{2r^2} - \frac{A_{Ham} A}{4\pi r^3} + \frac{k}{2} = 0 \tag{9}$$

Equations (8) and (9) form a system of non-linear equations which can be simplified by adding the two equations and defining the solution to be $r = g_{pi}$. The resulting equation is:

$$-\frac{\pi^2 \hbar c A}{120 g_{pi}^4} - \frac{A_{Ham} A}{6\pi g_{pi}^3} - 2kg_0 + 3kg_{pi} = 0 \tag{10}$$

The above expression can be solved numerically to obtain g_{pi}. Equation (8) can then be rearranged to calculate the pull-in voltage in terms of g_{pi}.

$$V_{pi} = \sqrt{\frac{2g_{pi}^2}{\varepsilon_o A}\left(k(g_o - g_{pi}) - \frac{A_{Ham} A}{6\pi g_{pi}^3} - \frac{\pi^2 \hbar c A}{240 g_{pi}^4}\right)} \tag{11}$$

When the initial gap is comparable to the width of a switch, the fringing field effect is significant. As the ratio of the gap to width increases, so does the influence of the fringing field on the pull-in voltage and thus, its effect should be modeled into the

pull-in equation. The electrostatic force with a first order fringing field correction F_{felec} is given by:

$$F_{felec}(r) = \frac{\varepsilon_o A V^2}{2r^2}\left(1 + \frac{0.65r}{w}\right) \tag{12}$$

Using the modified electrostatic force term, we obtain a new system of non-linear equations which can be solved numerically for g_{pi} and V_{pi}.

$$\frac{\pi^2 \hbar c A}{240 g_{pi}^4} + \frac{A_{Ham} A}{6\pi g_{pi}^3} + \frac{\varepsilon_o A V^2}{2 g_{pi}^2}\left(1 + \frac{0.65 g_{pi}}{w}\right) - k(g_o - g_{pi}) = 0 \tag{13}$$

$$-\frac{\pi^2 \hbar c A}{60 g_{pi}^4} - \frac{A_{Ham} A}{2\pi g_{pi}^3} - \frac{\varepsilon_o A V^2}{g_{pi}^2}\left(1 + \frac{0.65 g_{pi}}{2w}\right) + k g_{pi} = 0 \tag{14}$$

Results and Discussion

A cantilever beam and a fixed-fixed beam were chosen to represent the design of a NEM switch. Nominal dimensions of the beams were set to a width of 30 nm and a thickness of 20 nm with an initial gap of 20 nm between the electrodes. Length of the beam was varied from 200 nm to 1000 nm. The effect of each geometry parameter, namely width, thickness and initial gap, on the pull-in parameters was studied in detail.

The variation of the pull-in voltage of the switch with length was investigated using three different models. Figure 2 shows the pull-in parameters for cantilever and fixed-fixed beams for the following three cases:

(a) MATLAB: This is an analytical model that considers the short-range forces and the fringing electrostatic force. This model, represented by equations (13) and (14), was numerically evaluated in MATLAB.

(b) COMSOL: This is a full 3D FEM simulation in COMSOL Multiphysics software with coupled mechanical and electrostatic domains. Fringing field effect is also included in 3D simulations. However, the model for short-range forces is not a standard part of any FEM software package. Hence, equations (1) and (2) were manually added as pressure on the beam surface.

(c) COMSOL ES ONLY: As in case (b), this is a full 3D FEM simulation but without the addition of short-range forces. This model represents the traditional method of simulating NEM switches and serves as a benchmark in this study.

The analytical equations have been derived using an SDOF lumped model that does not take the variation of gap along the beam length into account. The COMSOL model automatically captures this effect and hence, a discrepancy between these two models was expected.

In figure 2 it is observed that all three models yield similar pull-in voltages when the beams are shorter. As the beams get longer, there is a significant divergence from the simple electrostatic model. This divergence can be attributed to the fact that longer beams are more compliant and hence more susceptible to short-range forces. Cantilever beams, which are more compliant than the fixed-fixed beams, strongly express this behavior. This effect is captured by both analytical and FEM models. This is a confirmation that short-range forces can significantly influence the design space for NEM switches.

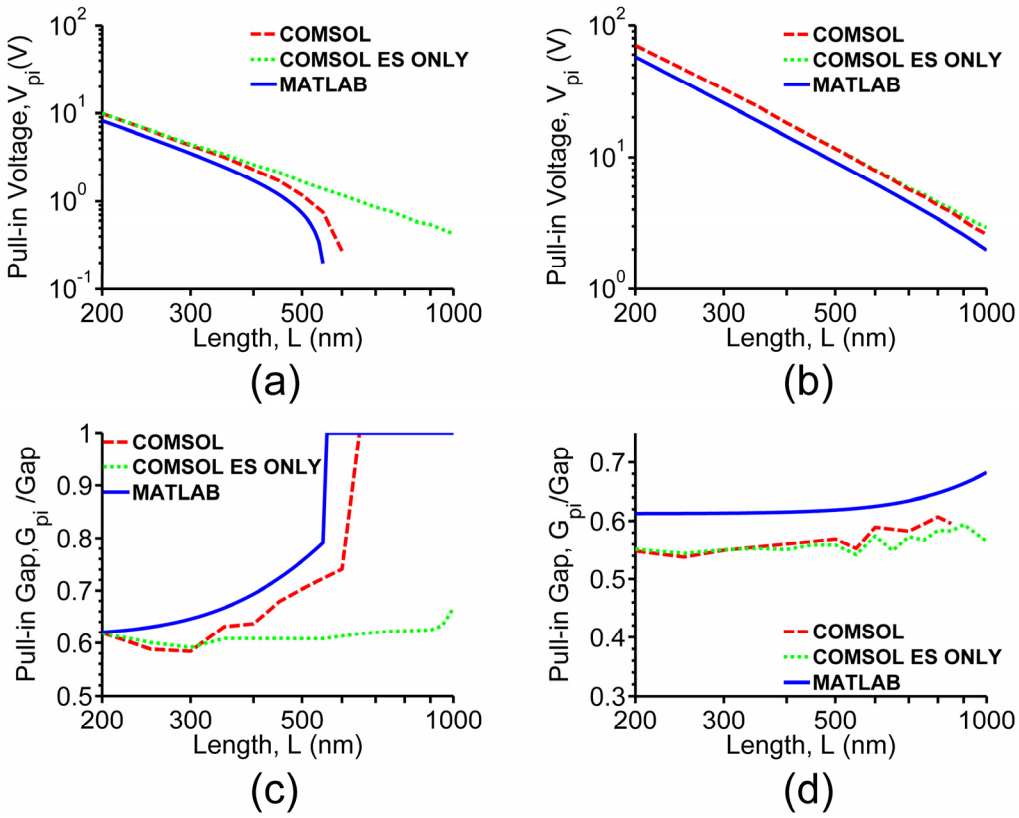

Figure 2: Comparison between analytical and FEM models for beam dimensions w = 30 nm, t = 20 nm and gap = 20 nm. (a) Pull-in voltage as a function of length for cantilever beam (b) Pull-in voltage as a function of length for fixed-fixed beam (c) Pull-in gap as a function of length for cantilever beam (d) Pull-in gap as a function of length for fixed-fixed beam

While the analytical equations correctly capture the trend in cantilever and fixed-fixed beams, there is a disparity between MATLAB and FEM results. This discrepancy comes from the assumption in SDOF lumped parameter model where the electrodes remain parallel instead of taking a bent shape. This means that in the analytical model, the effect of the short-range forces is stronger. Despite the difference, the analytical model is still useful because it captures all the important pull-in characteristics. This allows for faster search of design space when designing a

NEM switch. Once the design space is narrowed down, an accurate analysis should be carried out using a more extensive FEM model.

Another important observation comes from the analysis of pull-in gap shown in figure 2(c) and 2(d). Similar to the analysis of pull-in voltage, stiffer beams have almost identical critical pull-in gaps in all three models. However, as the beam becomes more compliant, the effect of short-range forces becomes significant. In the case of the cantilever switch where the contribution from the short-range forces was ignored, increasing length has no effect on the critical pull-in gap and hence a design of any length would be allowed. However, when all the forces are considered, there exists a maximum length of the beam beyond which the beam becomes mechanically unstable and would pull-in without any applied voltage. The fixed-fixed design on the other hand does not have this automatic pull-in problem for the lengths considered.

Based on these simulation results, fixed-fixed design is better suited for NEM applications. The effects of these short-range forces in a fixed-fixed design are minimal and can be neglected. However, because of the higher stiffness associated with such designs, the required pull-in voltage will be higher. Whenever the large pull-in voltage is a concern and application calls for a compliant structure, the short-range forces must be accounted for.

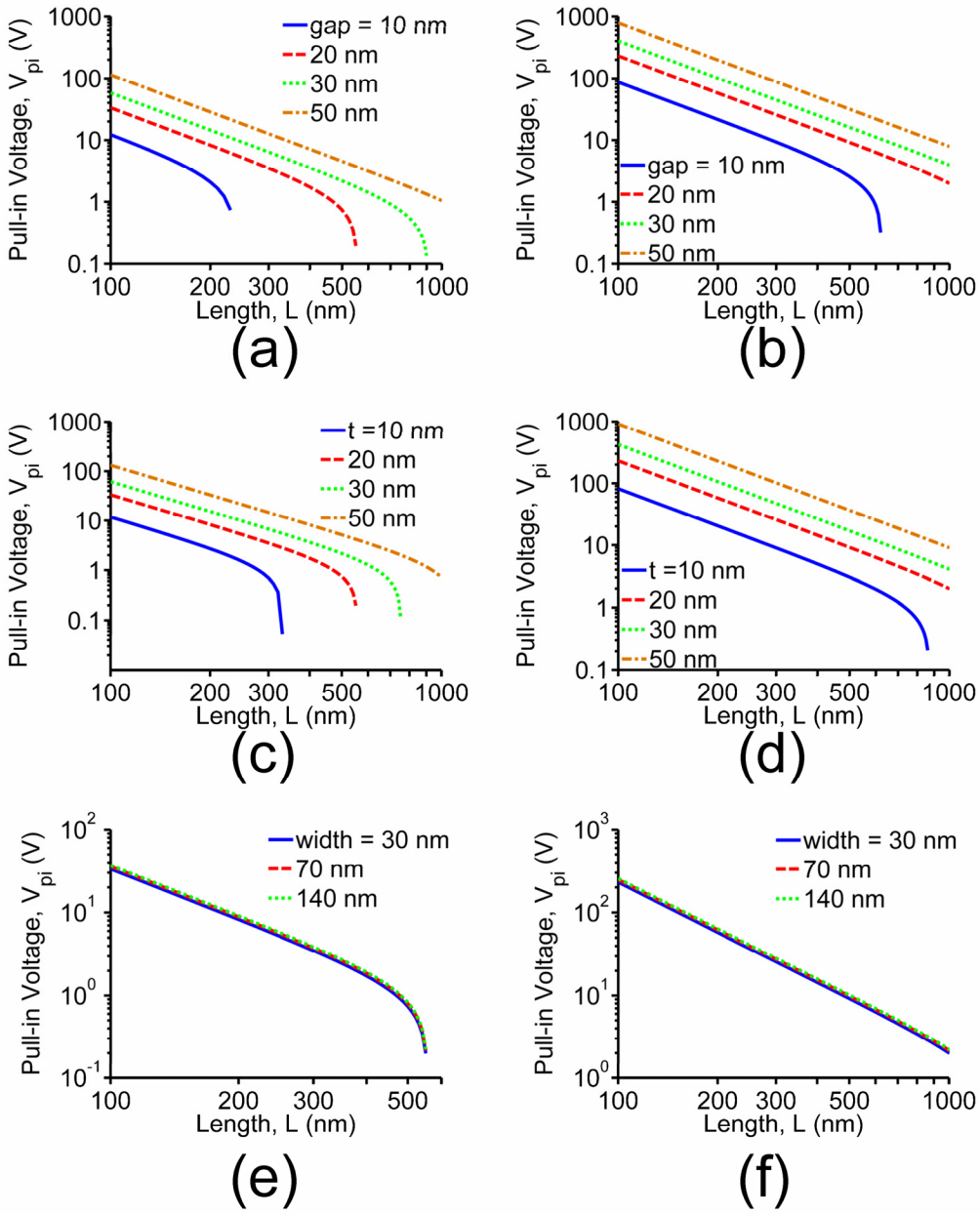

Figure 3: Parametric analysis of pull-in voltage using analytical model for beam dimensions w = 30 nm, t = 20 nm and gap = 20 nm. (a) Effect of gap variation on cantilever beam (b) Effect of gap variation on fixed-fixed beam (c) Effect of thickness variation on cantilever beam (d) Effect of thickness variation on fixed-fixed beam (e) Effect of width variation on cantilever beam (f) Effect of width variation on fixed-fixed beam.

The results of parametric analyses of the pull-in voltage using the analytical model for a cantilever beam are shown in figure 3(a), 3(c) and 3(e) and that for fixed-fixed beam are shown in figure 3(b), 3(d) and 3(f). Only one parameter was varied at a time to study its isolated effect on the pull-in voltage. Plots with gap and thickness variations show that these parameters can give some flexibility in the maximum length of the beam while keeping the pull-in voltage reasonably small. Varying the width however had very little effect as expected because all the forces are linearly proportional to it. The fringing fields of electrostatic force, which depend on the width, are not significant for this particular beam geometry.

Since the above geometry does not capture the effect of fringing fields, a new geometry was studied that emphasizes their effect. From the equations of SODF model it can be found that the fringing fields will affect the geometries with large gap to width ratio. Figure 4(a) and 4(b) show that both cantilever and fixed-fixed beams are similarly affected by the fringing field as the width is varied for a fixed gap. All short-range forces are included in this analysis.

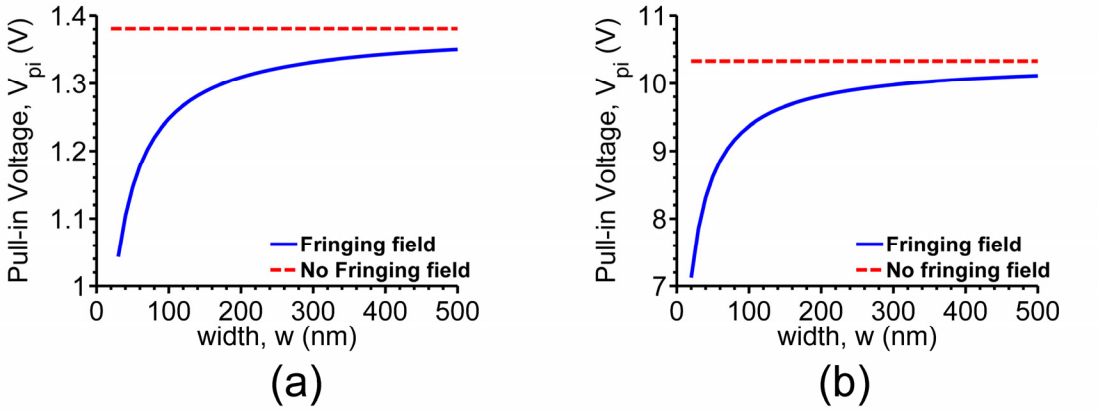

Figure 4: Effect of fringing field in the analytical model for beam dimension L = 1000 nm, t = 20 nm and gap = 50 nm. (a) Pull-in voltage as a function of width for cantilever beam (b) Pull-in voltage as a function of width for fixed-fixed beam.

The degree to which the pull-in voltage is affected depends on the geometry chosen and in some case it can be neglected, but as shown in the case below it can change the pull-in voltage up to 40%. Therefore, this correction term should be considered and leveraged when designing a NEM switch. This is particularly helpful for fixed-fixed beams because of the higher pull-in voltage associated with such devices.

CHAPTER 3

BEAM DYNAMICS

In some applications of NEM switches, specifically memory applications, the switching and release times are important characteristics that determine the write and read speed of the memory. In this chapter, the effect of short-range forces on the pull-in and pull-out times is studied using a SDOF lumped parameter model. In dynamic modeling, the effect of the repulsive van der Waals force is important and is therefore accounted for in this study. The repulsive force acts over a very small range and becomes dominant when the gap becomes small. This can cause bouncing of the beam and lead to longer settling time. The effect of van der Waals force on the dynamics of a cantilever based micro-switch has been studied by Granaldi at al. in [17]. Their study does not consider the release behavior of the beam, which is equally important because the release time together with the switching time determines the maximum frequency at which the switch can be operated. They also do not take into account the influence of Casimir force which can change the dynamic characteristics significantly. Here, the switching and release times of cantilever and fixed-fixed beams are studied with and without Casimir force.

Theory

The dynamic equation of motion based on an SDOF lumped parameter model for a NEM switch is described by a second order non-linear differential equation:

$$m_{eff}\frac{d^2x}{dt^2} + b\frac{dx}{dt} + kx = F(x)_{felec} + F(x)_{vdW} + F(x)_{cas} \tag{15}$$

where x is the tip displacement, m_{eff} is the effective modal mass of the beam, b is the damping factor and k is the spring constant of the beam.

For systems in vacuum, damping factor is influenced primarily by the structural losses and is dependent on the quality factor Q. The Q of the beam can change the dynamics considerably and hence is an important design parameter. Equation (15) can be rewritten in terms of Q and resonant frequency ω_0 where $Q = \sqrt{km_{eff}} / b$ and $\omega_o = \sqrt{k / m_{eff}}$. The effective modal mass m_{eff} is a function of type of force loading and the boundary conditions on a beam. The effective modal mass of 0.6471·m for cantilever beam and 0.7671·m for fixed-fixed beam [18] was used in this study (where m is the actual mass of the beam).

$$\frac{d^2x}{dt^2} + \frac{\omega_o}{Q}\frac{dx}{dt} + \omega_o{}^2 x = \frac{F_{elec} + F_{vdw} + F_{cas}}{m_{eff}} \tag{16}$$

Equation (16) can be used to study the switching time when the initial conditions for displacement and velocity are set to zero. To model the release time, the electrostatic force F_{felec} is set to zero in addition to setting the initial condition for displacement to gap and velocity to zero.

Switching Time: Results and Discussion

Equation (16) was numerically integrated in MATLAB under two conditions: (1) with Casimir and (2) without Casimir force. Case (1) where the Casimir force is neglected is used as a benchmark for comparison with case (2) which includes Casimir force. The effect of quality factor Q of the beam was considered to determine the switching time t_o at which the beam makes its first contact with the substrate.

Case (1): No Casimir Force

When the contribution of Casimir force on the switch is neglected an under-damped response is observed as the beam hits the substrate. As a result there is a time Δt between the first instance of contact t_o and the steady state. The amplitude of the bounce is a function of the quality factor, as expected.

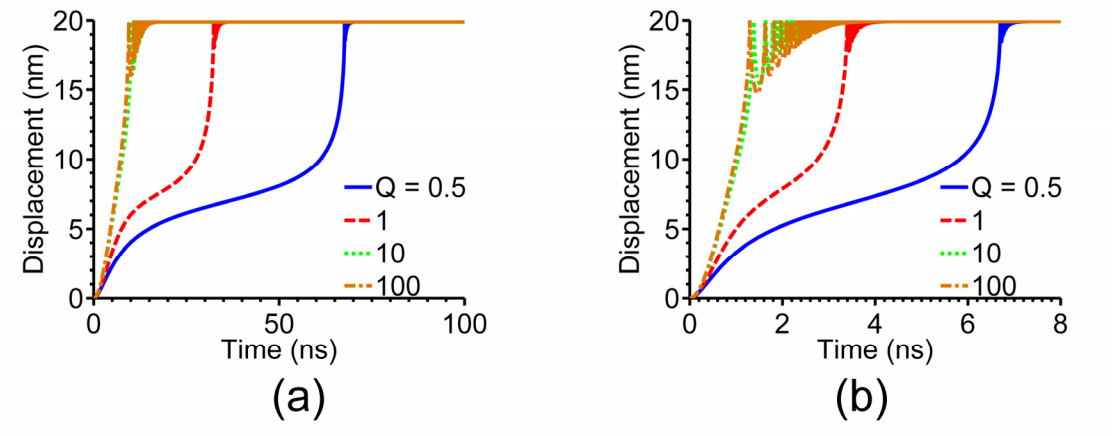

Figure 5: Dynamic pull-in response without Casimir force for different quality factors for beam dimension L = 400 nm, w = 30 nm, t = 20 nm, gap = 20 nm. (a) Displacement as a function of time for cantilever beam of resonant frequency 66.3 MHz and period 15.1 ns (b) Displacement as a function of time for fixed-fixed beam of resonant frequency 459.4 MHz and period 2.2 ns.

When a voltage higher than the pull-in voltage is applied, the beam will touch the substrate at time t_o. Figure 5 shows the dependence of switching time t_o to the quality factor. A higher quality factor means that the beam loses less energy to the environment and this directly translates to faster switching times. Figure 5 also shows that very high Qs do not have much effect on t_o while lower Qs can make more difference. There is no real advantage of having quality factors higher than 10. As Q increases, the switching time approaches half of the resonant frequency period. Therefore as observed in figure 5, the stiffer fixed-fixed beams with higher resonant frequency have much shorter switching times compared to the more compliant cantilever beams when their respective pull-in voltages are applied.

When there is no Casimir force, the repulsive forces compete with the attractive forces. Due to their magnitudes being relatively equal in the range of displacements considered, a characteristic bouncing of the beam is observed until a

steady state is reached. The amplitude and duration of the bounce is correlated to the quality factor. When the quality factor is high, only a small amount of the energy is lost in each collision and therefore, the amplitude of the bounce is higher and the beam oscillations die out slower. An interesting observation of the bouncing shows that the frequency of the bounce increases as the oscillation dampens out in magnitude. This is mostly due to nonlinearity of the forcing function.

Case (2): With Casimir Force

The bouncing behavior observed above is completely eliminated with the addition of Casimir force as the attractive forces overpower the repulsive forces. The displacement as a function of time in Figure 6 shows this effect more clearly. As previously observed, there is no advantage to having a system with high *Q*. Figure 6 shows that between Q= 10 and 100 there is little difference in switching time. However, between Q = 0.5, 1, and 10 there is a significant improvement in switching time from 58 ns to 9 ns for cantilever and 8.7 ns to 1.3 ns for fixed-fixed beams.

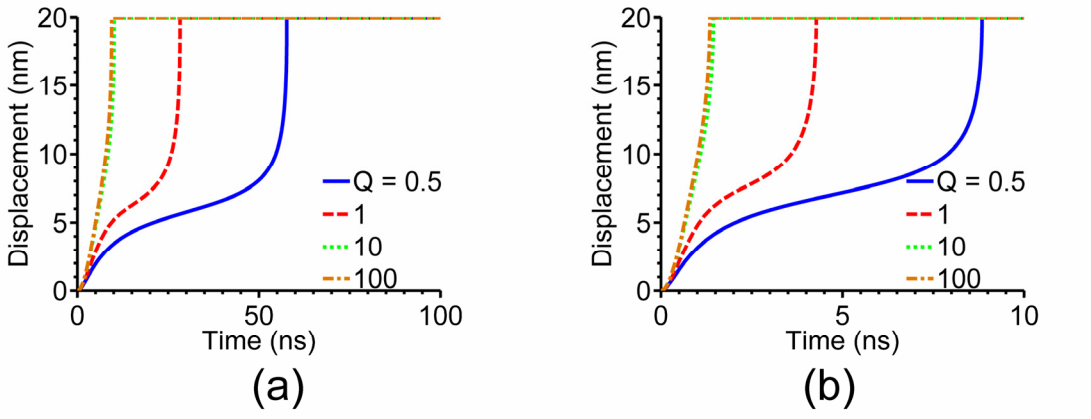

Figure 6: Dynamic pull-in response with Casimir force for different quality factors for beam dimension L = 400 nm, w = 30 nm, t = 20 nm, gap = 20 nm. (a) Displacement as a function of time for cantilever beam of resonant frequency 66.3 MHz and period 15.1 ns (b) Displacement as a function of time for fixed-fixed beam of resonant frequency 459.4 MHz and period 2.2 ns.

Figure 7 shows the switching time for different ratios of the applied voltage to the pull-in voltage for varying *Q*s. There is a benefit of reduced switching time as the ratio is increased to some extent. However, to keep the applied voltage at a reasonable number, a ratio of 1.2-1.4 is perhaps ideal. It is possible to reduce the dynamic pull-in voltage even further than the static case by increasing the quality factor. As *Q* gets higher, the inertia makes it easier for the beam to go past the critical pull-in gap and hence to get pulled in earlier.

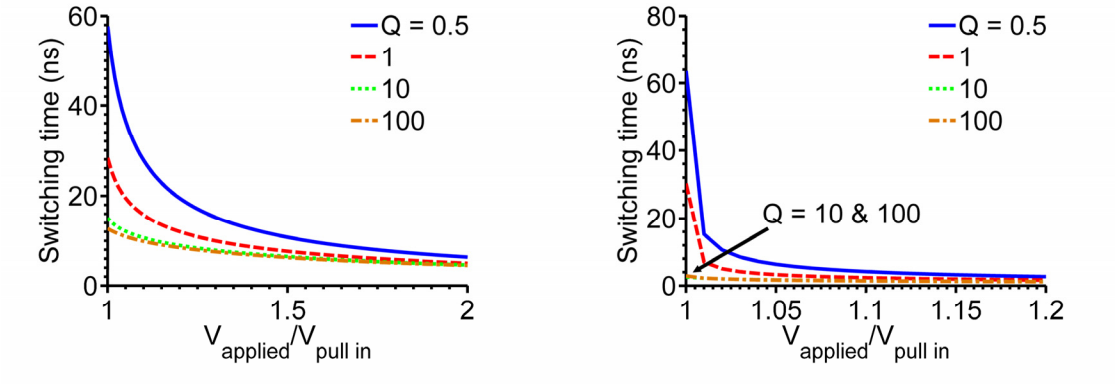

Figure 7: Effect of applied voltage on the switching time for different quality factors for beam dimension L = 400 nm, w = 30 nm, t = 20 nm, gap = 20 nm. (a) Switching time as a function of ratio of applied voltage to pull-in voltage for cantilever beam (b) Switching time as a function of ratio of applied voltage to pull-in voltage for fixed-fixed beam.

Release time: Results and Discussion

Since the electrostatic force is no longer active, it is the effect of the Casimir, van der Waals and spring restoring forces that determine the release response. When the initial condition of the displacement is set to the gap, the attractive forces theoretically blow up to infinity and the beam would never release. In practice this

corresponds to in-use stiction. However, due to the roughness of the material, the gap is always larger than a few lattice constant of the material (0.1-0.5 nm). Therefore the beam should be designed such that it can pull out from the initial gap that is in the order of magnitude of material roughness. Smart designs with realistic geometries that can cleverly avoid stiction are suggested in the next few sections. Using the same geometry as for the switching time, the pull out of the beam was simulated for two cases: (1) without Casimir and van der Waals force, (2) with Casimir and Van der Waals forces.

Case (1): With only the spring restoring force acting, the beam was able to pull out when the voltage was turned off. This simulation shows the ideal pull out time if there were no stiction in the design. Figure 8 depicts that the beam released itself from the displacement of 20 nm back to 0 nm and the time taken to settle down to a steady state value is very much a function of Q. A Q of 1 is a good value that that gives a critically damped response with small overshoot and fast release and settling time.

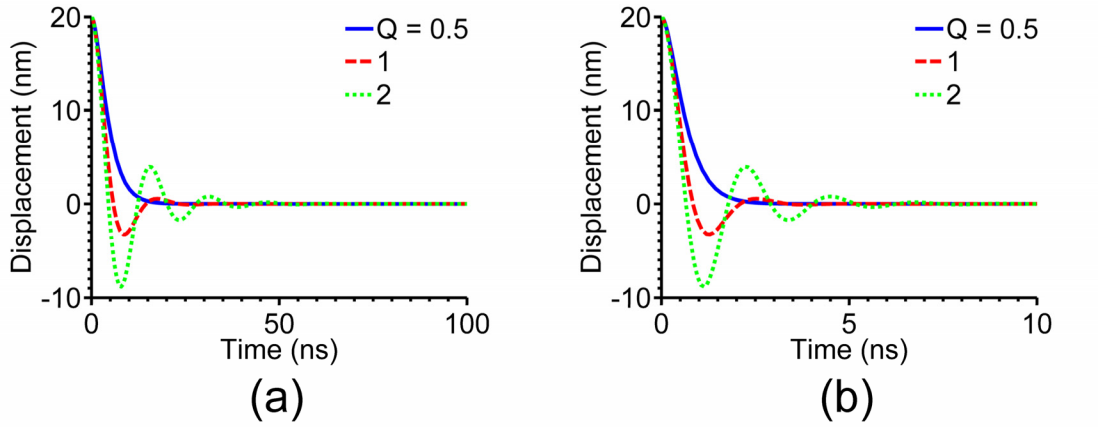

Figure 8: Dynamic pull-out response without short-range forces for different quality factors for beam dimension L = 400 nm, w = 30 nm, t = 20 nm, gap = 20 nm. (a) Displacement as a function of time for cantilever beam (b) Displacement as a function of time for fixed-fixed beam.

Simulating Qs larger than 2 results in larger overshoot and long settling times, which are not desirable characteristics for NEM switches. This is in contrast to the observation in the previous section, where Q as large as 10 was preferable to obtain fast switching times. This trade off means that the quality factors should not be higher than 2 to have both switching and release times small. With a Q of 1, the settling of the beam takes just over one half of natural frequency period. The overall actuation frequency of the NEM switch in this case would approach the natural frequency.

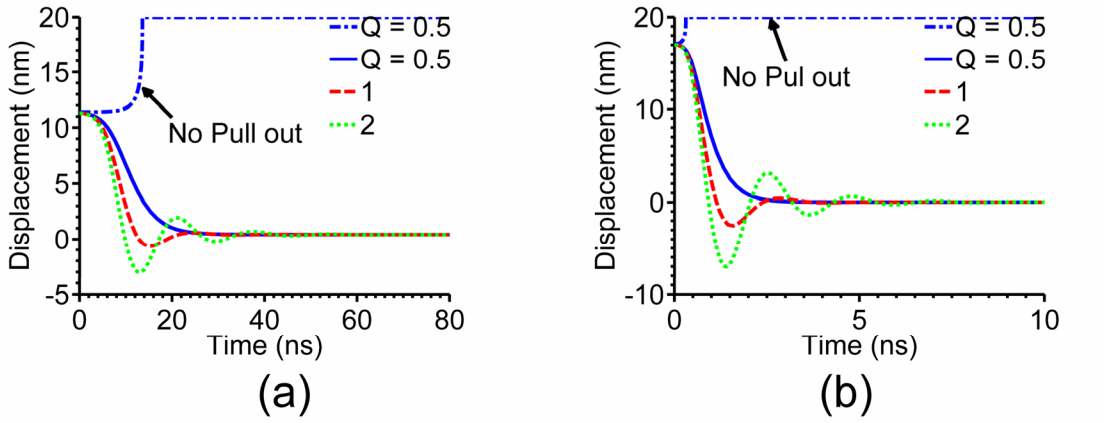

Figure 9: Dynamic pull-out response with short-range forces for different quality factors for beam dimension L = 400 nm, w = 30 nm, t = 20 nm, gap = 20 nm. (a) Displacement as a function of time for cantilever beam (b) Displacement as a function of time for fixed-fixed beam.

Case (2): When the short-range forces were added, the pull out behavior was completely altered. Figure 9(a) and 9(b) show that when the beam undergoes a displacement of more than 11.3 nm for cantilever and 17 nm for fixed-fixed beam (for an initial gap of 20 nm), the attractive forces dominate and the beams cannot pull out. If the beams are released from smaller initial displacements, they can overcome the short-range forces and fully restore. The release times are still comparable to case (1),

resulting in an actuation frequency that is on the order of natural frequency of the beam.

Failure to pull out is a common problem in NEM devices and as it is shown in this section, it is correlated to the short-range forces. The approach to counter the problem is either by increasing the repulsive force or using smart geometries. This can be achieved in several ways: (1) increasing the spring constant, (2) applying electrostatic force in the opposite direction and (3) adding a dimple at the bottom of the beam at the contact location.

If the spring constant method is chosen, varying the length and thickness of the beam is most effective in controlling the stiffness. However, as the beam becomes stiffer the trade off will be the higher voltage required to pull-in. Some of the increase in the electrostatic force needed can be compensated by making the width few orders smaller than the gap so that the fringing component of the electrostatic force can be used. The second method involves a more complex structure like a torsion beam where a voltage can be applied to one side to pull the other side up. However, this design is more prone to instability. An alternative to the torsion beam is a bridge structure that places an additional electrode on top of the beam. However, this type of design presents fabrication and modeling challenges. The third method of adding a dimple at the edge of the beam to prevent the switch from completely collapsing is commonly mentioned. In addition to fabrication challenges, the dimple design suffers from reduced contact resistance.

CHAPTER 4

APPLICATIONS

Dynamic Random Access Memory (DRAM)

The scaling of CMOS devices into nanometers has produced several challenges such as short channel effects, junction leakage and gate oxide leakage in the semiconductor industry [19, 20]. A NEM device is a promising solution to replace one transistor and one capacitor based memory cell because of almost zero off current, very high sub-threshold slope, fast switching times and small cell size. NEM devices also enjoy the advantage of improved robustness to temperature variation and external radiation. In this section, the application of NEM switch as a memory element for DRAM is discussed.

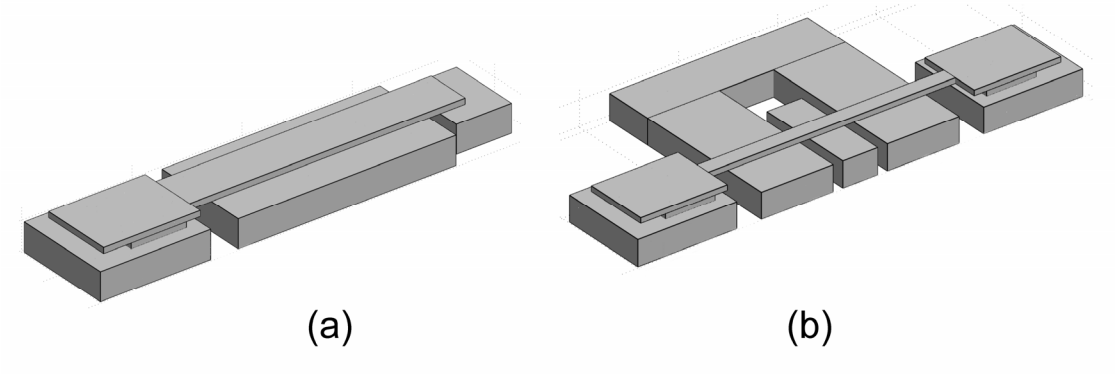

Figure 10: 3D model of NEM DRAM cell. (a) Cantilever based switch (b) Fixed-fixed based switch.

DRAM: Results and Discussion

Because of the varying force distribution applied on the beam due to the electrode arrangement, there is no straightforward analytical solution to the pull-in parameters of the beam designs shown in figure 10. Therefore, the 3D models were simulated in COMSOL Multiphysics to determine the pull-in voltage as a function of

length for different widths considering all the short-range forces. The results of the simulation are shown in figure 11 and they indicate that beams with shorter widths are preferable to keep the pull-in voltage small at about 1 V. If only electrostatic forces are considered, a gap of 10 nm would be sufficient for both cantilever and fixed-fixed structures. However, in reality with the addition of Casimir and van der Waals forces, the cantilever structures need a gap of at least 25 nm to avoid automatic pull-in, while the fixed-fixed structures require a gap of at least 16 nm.

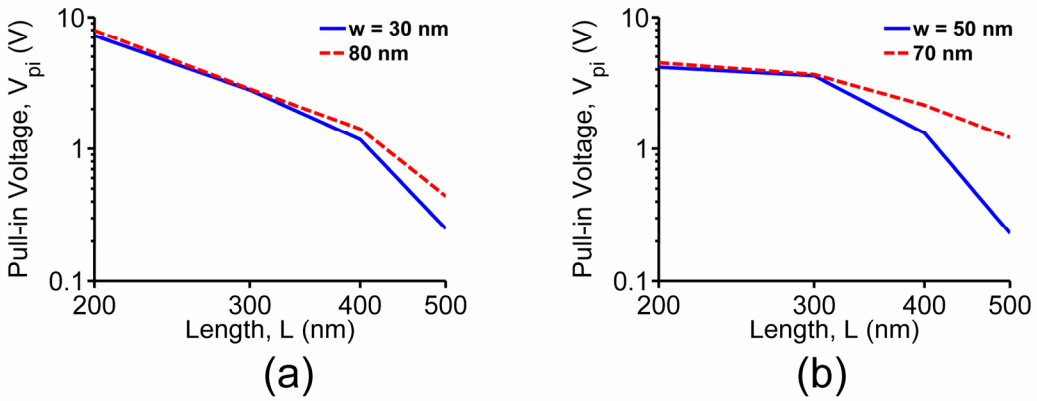

Figure 11: Parametric analysis of pull-in voltage using FEM model considering all short-range forces. (a) Effect of width variation in cantilever beam for gap = 25 nm and t = 10 nm (b) Effect of width variation in fixed-fixed beam for gap = 16 nm and t = 10 nm.

The pull-out simulation for these beams is more complex because it involves setting up a dynamic simulation in FEM software with specific initial conditions. Therefore, a static simulation was first performed by forcing a prescribed displacement equivalent to the gap on the tip of the beam. The static solution was then used as the initial condition for a transient simulation where all the short-range forces were added. This set up is essentially the equivalent of a dynamic simulation and provides the displacement of the beam as it is pulled up as a function of time. It was

interesting to find that not all of the geometries discussed above can pull out. In fact only cantilever beams with carefully placed electrodes can pull out while requiring relatively low pull-in voltages. A summary of the simulation results for cantilever beam are given in table 1.

Table 1: Release response of cantilever beam showing switching time.

	L = 200nm	*L = 300nm*	*L = 400nm*	*L = 500nm*
w= 30nm	3.8ns	11.6ns	No pull-out	No pull-out
w = 80nm	3.6ns	11.4ns	No pull-out	No pull-out

As table 1 shows longer beams are too compliant to release on their own while shorter ones have a reasonable settling time for *Q* of about 1. If the beams are made wider, there is a small gain in settling time due to a small increase in stiffness.

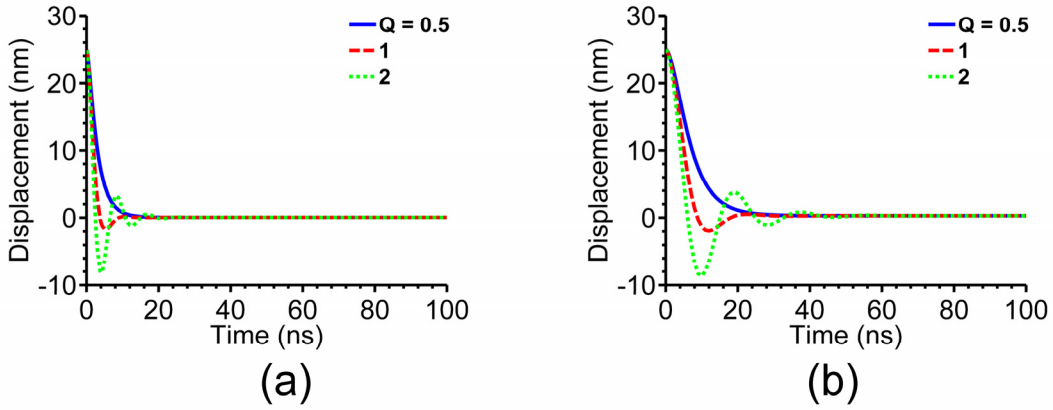

Figure 12: Dynamic pull-out response of NEM DRAM memory cell with all short-range forces for different quality factors for cantilever beam dimension w = 80 nm, t = 10 nm, gap = 25 nm. (a) Length = 200 nm (b) Length = 300 nm

Figure 12 shows the release behavior of a cantilever NEM switch for different *Q*s. The fastest release time is 3.6 ns for the beam with length of 200 nm and 11.4 ns

for the beam with length of 300 nm when their Q is set to 1. The respective actuation frequencies of a memory switch based on these particular designs would be 0.12 GHz and 43.8 MHz with the corresponding pull-in voltages of 7.94 V and 2.8 V. The results here clarify the trade off between designs that are fast but at the same time work with low applied voltage.

Electric Field Sensor

Electrical equipments, power lines, communication signals, etc generate small electric fields over a wide range of frequencies. Detecting these small electric fields over a large range of frequencies is very challenging. Conventionally, an electric field is sensed using a combination of an antenna and a receiver. However, in such systems it is not possible to get both high sensitivity and broad frequency response, both of which scale with antenna size. Therefore, there is a need for a compact small electric field detector that has both high sensitivity and wide frequency response.

Draper Laboratory [21] has proposed a hybrid antenna system that amplifies inputs from a traditional antenna by integration with a NEM resonator. The concept simply uses the small charge generated by the external electric field at the antenna to mechanically amplify the motion of the resonator. This hybrid NEMS-antenna based electric field detector clearly has the advantages of a small form factor, high sensitivity ($0.1\,\mu V/m\sqrt{Hz}$) and high in-band signal amplification and out of band signal rejection. Each resonator could be given some tunability and an array of such resonators could be used to cover the range of frequencies needed for wide band operation.

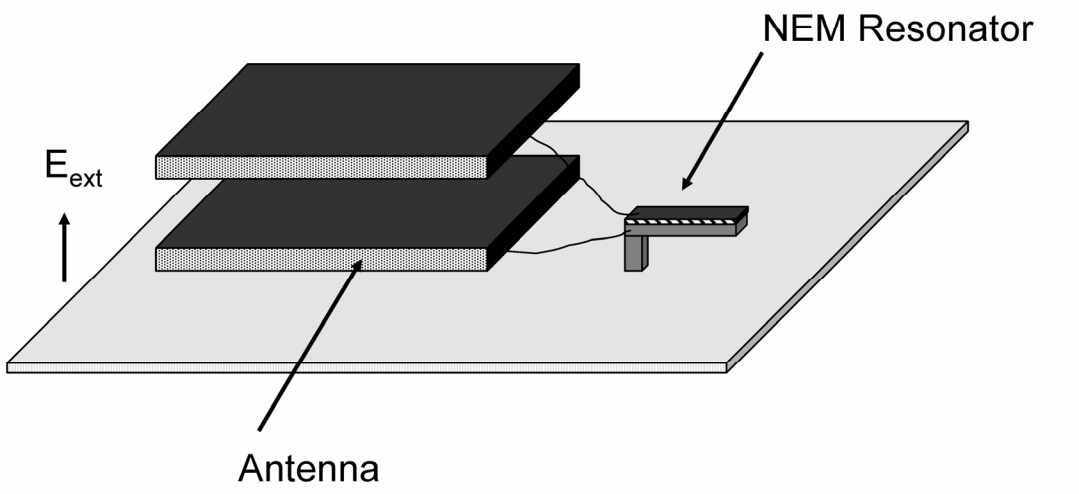

Figure 13: The concept of the hybrid NEMS-antenna based electric field sensor.

The NEM resonator shown in figure 13 can be any type of resonator. In this study a piezoelectric resonator is considered as a suitable candidate because of the large displacement amplitudes that can be achieved without applying any DC bias normally required by other types of resonators. A piezoelectric resonator consists of a NEM switch with a thin layer of piezoelectric material deposited on the top surface, followed by a thin electrode. The switch itself acts as a bottom electrode for the piezoelectric layer. As a time varying voltage is applied across the piezoelectric material, stress develops inside it stretching or compressing the top surface of the beam. This causes the beam to deform and when the excitation frequency matches the resonant frequency of the structure, the deformation is mechanically amplified. Lead zirconium titanate (PZT) is chosen as the piezoelectric material for the resonator because it has a very high piezoelectric coefficient d_{31} and hence produces the largest displacement for a given input voltage.

The total charge Q_{tot} generated across the hybrid mechanical antenna for a given external electric field E_{ext} is given by Gauss' law:

$$Q_{tot} = Q_A + Q_R = \varepsilon_o E_{ext} A_A + \varepsilon_{PZT} E_{ext} A_R \tag{18}$$

where, Q_A and Q_R are the charge collected across the antenna and the resonator respectively, A_A and A_R are the areas of the antenna and the resonator respectively and ε_{PZT} is the dielectric constant of PZT.

It follows that the total voltage V_{tot} across the resonator is:

$$V_{tot} = \frac{Q_A + Q_R}{C_A + C_R} \tag{19}$$

where, C_A and C_R are the capacitances of the antenna and the PZT layer of the resonator. Equation (19) can be expanded to the following equation:

$$V_{tot} = E_{ext} g_A \frac{1 + \dfrac{\varepsilon_{pzt}}{\varepsilon_o} \dfrac{A_R}{A_A}}{1 + \dfrac{\varepsilon_{pzt}}{\varepsilon_o} \dfrac{A_R}{A_A} \dfrac{g_A}{t_{pzt}}} \tag{20}$$

where, g_A is the gap between the antenna electrodes and t_{PZT} is the thickness of the PZT layer. The voltage produces a static displacement [22], $x_{R\text{-}Static}$ of the bimorph beam and is given by:

$$x_{R-Static} = \frac{a_1 a_2}{a_3} 3 d_{31} L^2 V_{tot} \tag{21}$$

where a_1, a_2 and a_3 are constants defined as following:

$$a_1 = E_{Si} E_{pzt} \left(E_{pzt} t_{Si} + E_{Si} t_{pzt} \right)$$

$$a_2 = \frac{t_{Si} \left(t_{Si} + t_{pzt} \right)}{E_{pzt} t_{Si} + E_{Si} t_{pzt}}$$

$$a_3 = 4E_{pzt}E_{Si}t_{Si}t_{pzt}^{3} + 4E_{pzt}E_{Si}t_{Si}^{3}t_{pzt} + E_{pzt}^{2}t_{Si}^{4} + E_{Si}^{2}t_{pzt}^{4}$$

$$+ 6E_{pzt}E_{Si}t_{Si}^{2}t_{pzt}^{2}$$

where, E_{PZT} and E_{Si} are elastic moduli of PZT and silicon (structural material of the resonator) respectively and t_{PZT} and t_{Si} are the thickness of PZT layer and silicon respectively.

From the equation of motion for a harmonic resonator, vibration amplitude as a function of the excitation frequency ω is given by:

$$|X| = \frac{x_{R-Static}k_c/m_c}{\sqrt{\left(\omega^2 - \omega_o^2\right)^2 + \left(\omega\omega_o/Q\right)^2}} \tag{23}$$

where, k_c is the spring constant and m_c is the effective mass of the composite PZT-Silicon bimorph and ω_o is the natural frequency of the bimorph resonator.

At resonance, the displacement $x_{R\text{-}Dynamic}$ of the PZT resonator beam is:

$$x_{R-Dynamic} = Qx_{R-Static} \tag{22}$$

Since the resonator displacement is likely to be small, in the range of 10^{-15} to 10^{-18} m, the thermo-mechanical noise will limit the device performance. The thermo-mechanical noise [23] is given by:

$$x_n = \sqrt{\frac{4k_BTQ}{\omega_o k_c}} \tag{23}$$

where, k_B is Boltzmann's constant and T is the temperature.

The PZT resonator geometry can be optimized to achieve the resonator motion higher than the noise floor. Moreover, the noise floor itself may be reduced by averaging the uncorrelated noise in an array of resonators. Another alternative to

reducing the noise floor is lowering the temperature by laser cooling. The effects of some of these design parameters on the signal to noise ratio (SNR) of the hybrid antenna are investigated in the next section.

Electric field sensor: Results and Discussion

As figure 14 shows, shorter beams have higher resonant frequency and also an improved signal to noise ratio for the given geometry and conditions. However, for all lengths, the SNR only approaches 1 at resonance. So, the geometry itself must be optimized in order to obtain a better SNR. The results of the parametric analyses on some of the geometric parameters and environmental conditions are discussed below.

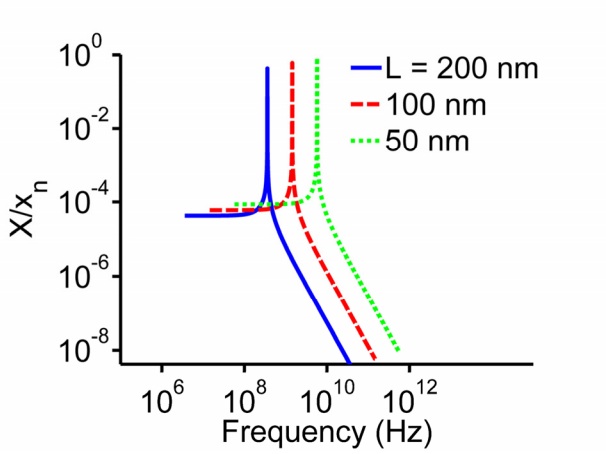

Figure 14: Frequency response of the PZT NEM resonator for varying lengths for Q = 10,000, w = 30 nm, t_{pzt} = 5 nm, t_{Si} = 10 nm, T = 300 K and E_{ext} = 0.1 uV/m.

The simulation results demonstrate how a variation of a single parameter affects the SNR. Figure 15 shows that length is not a critical a parameter for optimization. Length should be kept shorter but it is the width and the thickness of the silicon layer of the bimorph that should be optimized for better control of SNR. The ratio is also very sensitive to temperature because lower temperature can drastically

reduce the thermo-mechanical noise. Very high quality factor is harder to achieve but nevertheless, it is desirable to have a reasonably high *Q*.

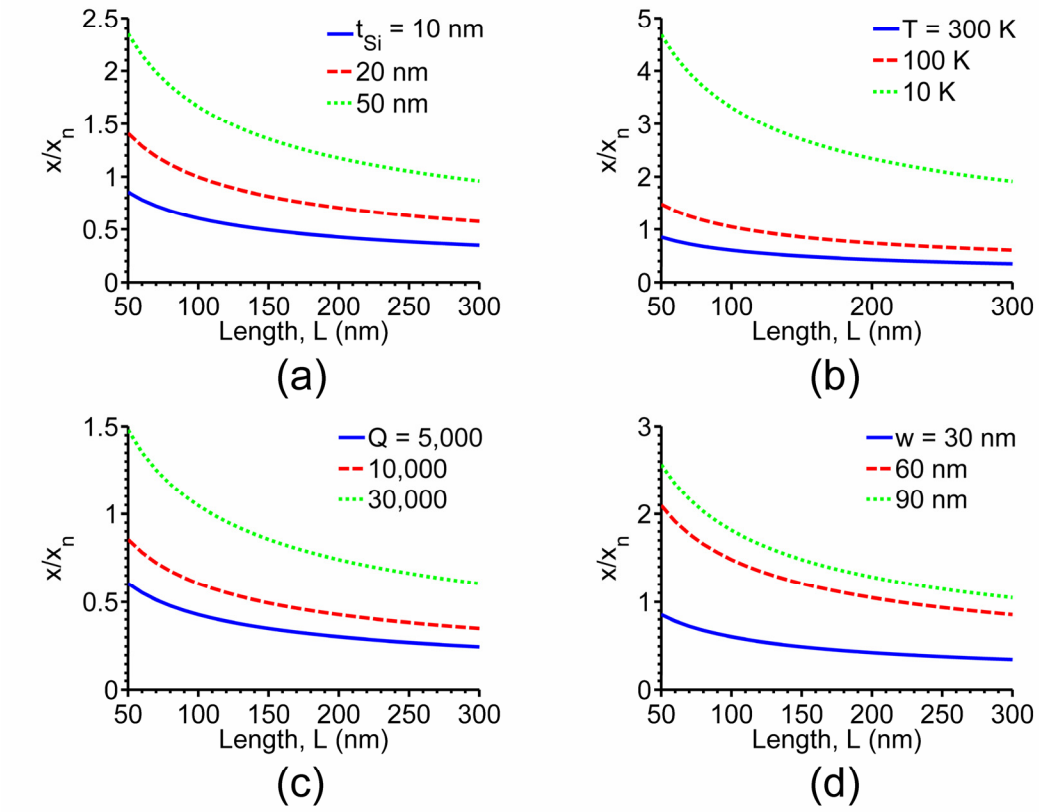

Figure 15: Parametric analysis of signal to noise ratio as a function of length for Q = 10,000, w = 30 nm, t_{pzt} = 5 nm, t_{Si} = 10 nm and T = 300 K. (a) SNR as a function of length for varying thickness of silicon beam (b) SNR as a function of length for varying temperature (c) SNR as a function of length for varying quality factor (d) SNR as a function of length for varying width.

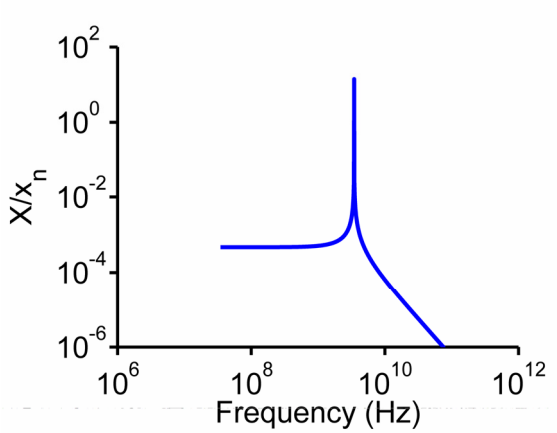

Figure 16: Frequency response of an ideal PZT resonator design.

An example of an ideal design of a PZT resonator with realistic geometry optimized using the results from figure 15 has a length of 100 nm, width of 50 nm, thickness of Silicon is 25 nm, Q of 30,000 and would operate at the temperature of 10 K. Such a design would have an SNR of 14 and would produce a displacement of 33 fm. The frequency response of this design showing a resonance at 3.5 GHz is depicted in figure 16.

CHAPTER 5

CONCLUSION

In recent years there has been much interest in nano-scale mechanical devices and their applications. The most fundamental structure in NEMS is the NEM switch. These switches have been extensively researched, mostly in the static domain. However there is a lack of a study that investigates the total effects of short-range forces that are significant at this scale. In electrostatically actuated NEM switches, the fringing field effect is also important because of comparable gap to width ratio. Here, a model for NEM switches that takes into account Casimir and van der Waals forces as well as fringing fields has been developed and studied in detail.

Simulation results show that the combination of short-range forces and fringing fields significantly alter the behavior of NEM switches. Compliant structures, which are generally more desirable because they operate at low voltages, are shown to be particularly affected. Using the traditional model instead of the proposed model could easily result in structures that are mechanically unstable and would collapse even during fabrication.

It has been shown that both analytical and FEM models can be used to predict the general behavior of NEM switches. Analytical models are specifically useful for quickly narrowing down the design space. FEM models on the other hand are more complex and time consuming. However, they provide more accurate results and should be used to simulate actual device designs.

Bouncing behavior of switches upon contact with the substrate has been observed experimentally in micro-scale switches [24]. However this study shows that at nano-scale where the short-range forces are more dominant, the bouncing behavior is completely suppressed. While this appears to be a desirable effect, it is actually the stiction that prevents the bouncing. This is confirmed by the dynamic release

simulations. In order to avoid stiction, a design should have a large effective gap between actuating electrodes even after the beam has collapsed.

Two practical applications of NEM switches have been discussed at length. The NEM switches for DRAM application were designed to operate at a frequency of 0.12 GHz and 43.8 MHz with actuation voltages of 7.94 V and 2.8 V respectively. It has been shown that this particular design will avoid stiction. The NEM electric field sensor application was demonstrated to have sensitivity high enough to detect 0.1 μV/m with SNR as high as 14.

APPENDIX

Material Properties

Table 2. Proprietary Material Properties

Symbol	Physical Meaning	Value	Units
E_{PM}	Young's Modulus	100	GPa
ρ_{PM}	Density	1E4	$kg \cdot m^{-3}$
υ_{PM}	Poisson's Ratio	0.33	1
σ_{PM}	Conductivity	1E5	$\Omega^{-1} \cdot cm^{-1}$

Table 3. Silicon Material Properties

Symbol	Physical Meaning	Value	Units
E_{Si}	Young's Modulus	170	GPa
ρ_{Si}	Density	2330	$kg \cdot m^{-3}$
υ_{Si}	Poisson's Ratio	0.33	1
$\varepsilon_{r\text{-}Si}$	Relative Permittivity	11.7	1

Table 4. PZT Material Properties

Symbol	Physical Meaning	Value	Units
E_{PZT}	Young's Modulus	60	GPa
ρ_{PZT}	Density	7500	$kg \cdot m^{-3}$
υ_{PZT}	Poisson's Ratio	0.33	1
$\varepsilon_{r\text{-}PZT}$	Relative Permittivity	3130	1
d_{31}	Piezoelectric Charge Coefficient	274E-12	$C \cdot N^{-1}$

Numerical Constants

Table 5. List of numerical constants

Symbol	Physical Meaning	Value	Units
ε_o	Permittivity of air	8.854E-12	$F \cdot m^{-1}$
h	Planck's constant	6.626E-34	$m^2 \cdot kg \cdot s^{-1}$
c	Speed of light	2.998E8	$m \cdot s^{-1}$
A_{Ham}	Hamaker's constant	2E-19	J
k_B	Boltzmann's constant	1.38E-23	$m^2 \cdot kg \cdot s^{-2} \cdot K^{-1}$
C_2	Repulsive constant	1E-80	$N \cdot m^7$

REFERENCES

[1] Osterberg PM, Senturia SD (1997) M-TEST: a test chip for MEMS material propert measurement using electrostatically actuated test structures. J Microelectromech Syst 6(2):107-118

[2] Bochobza-Degani O, Nemirovsky Y (2002) Modeling the pull-in parameters of electrostatic actuators with a novel lumped two degrees of freedom pull-in model. Sens Actuators A 97-98:569-578

[3] Israelachvil J N (1985), Intermolecular and Surface Forces, Academic Press

[4] Dequesnes M, Rotkin SV, Aluru NR (2002) Calculation of pull-in voltages for carbon nanotube-based nanoelectromechanical switches. Nanotechnology 13:120-131

[5] Rotkin SV (2002) Analytical calculations for nanoscale electromechanical systems. Electrochem Soc Proc 6:90-97

[6] van Spengen WM, Puers R, De Wolf I (2002) A physical model to predict stiction in MEMS. J Micromech Microeng 12:702-713

[7] Lin WH, Zhao YP (2003) Dynamic behavior of nanoscale electrostatic actuators. Chin Phys Lett 20:2070-2073

[8] Ramezani A, Alasty A, Akbari J (2006) Influence of van der Waals force on the pull-in parameters of cantilever type nanoscale electrostatic actuators. Microsyst Technol 12:1153-1161

[9] Casimir H B G (1948). Proc K Ned Akad Wet 51:793

[10] Serry FM, Walliser D, Maclay GJ (1998) The role of the Casimir effect in the static deflection and stiction of membrane strips in MEMS. J Appl Phys 84(50):2501-2506

[11] Chan HB, Aksyuk VA, Kleiman RN, Bishop DJ, Capasso F (2001) Quantum mechanical actuation of microelectromechanical systems by the Casimir force. Science 291:1941-1944

[12] Chan HB, Aksyuk VA, Kleiman RN, Bishop DJ, Capasso F (2001) Nonlinear micromechanical Casimir oscillator. Phys Review Lett 87(21):211-801

[13] Lin WH, Zhao YP (2005) Casimir effect on the pull-in parameters of nanoswitches. Microsyst Tech 11:80-85

[14] Lambrecht, A (2002) The Casimir effect: a force from nothing. Physicsworld.com. Retrieved on May 8, 2009

[15] Casimir HBG (1948) On the attraction between two perfectly conducting plates. Proc K Ned Akad Wet 51:793-6

[16] Granaldi A, Paolo D (2006) The dynamic response of resistive microswitches: switching time and bouncing. J Micromech Microeng 16:1108-1115.

[17] Young WC, Budynas R (2001) Roark's Formulas for Stress and Strain, McGraw-Hill.

[18] Inman DJ (2001) Engineering Vibration. Prentice Hall Inc.

[19] Meindl JD, Chen Q, Davis JA (2001) Limits on silicon nanoelectronics for terascale integration. Science 293:2044–9.

[20] Frank DJ, Dennard RH, Nowak E, Solomon PM, Taur Y, Wong HSP (2001) Device scaling limits of Si MOSFET's and their application dependencies. Proc IEEE 89:259–88.

[21] Duwal A, Weinberg M, Bernstein J, Tingley R, White D, Chaparala M (2009) SHARX: Small hybrid antenna for radios and artificial exterocepters. DARPA/MTO proposal.

[22] Smits JG, Choi W (1991) The constituent equations of piezoelectric heterogenous bimorphs. IEEE Trans on Ultrasonics, Ferroelectrics and Frequency Control 38(3):256-270

[23] Li M, Tang HX, Roukes ML (2007) Ultra-sensitive NEMS-based cantilevers for sensing scanned probe and very high frequency applications. Nature Nanotech 2: 114-120

[24] McCarthy B, Adams G, McGruer N and Potter D (2002) A dynamic model, including contact bounce, of an electrostatically actuated microswitch. J. Microelectromech. Syst. 11(3):276-283